Journal of Molecular Structure 1094 (2015) 246–253

Contents lists available at ScienceDirect

Journal of Molecular Structure

journal homepage: www.elsevier.com/locate/molstruc

Multinuclear NMR and crystallographic studies of triorganotin valproates and their *in vitro* antifungal activities

Bárbara P. de Morais [a], Geraldo M. de Lima [a,*], Carlos B. Pinheiro [b], Rosane A.S. San Gil [c], Jacqueline A. Takahashi [a], Daniele C. Menezes [d], José D. Ardisson [e]

[a] Departamento de Química, Universidade Federal de Minas Gerais, UFMG, Avenida Antônio Carlos 6627, Belo Horizonte, MG CEP 31270-901, Brazil
[b] Departamento de Física, Universidade Federal de Minas Gerais, UFMG, Avenida Antônio Carlos 6627, Belo Horizonte, MG CEP 31270-901, Brazil
[c] Instituto de Química, Universidade Federal do Rio de Janeiro, UFRJ, Avenida Athos da Silveira Ramos, 149, Cidade Univesitária, RJ CEP 21941-909, Brazil
[d] Departamento de Química, Universidade Federal de Viçosa, UFV, Avenida Peter Henry Rolfs s/n, Viçosa, MG CEP 36570-001, Brazil
[e] Centro de Desenvolvimento em Tecnologia Nuclear, CDTN/CNEN, Avenida Antônio Carlos 6627, Belo Horizonte, MG CEP 31270-901, Brazil

HIGHLIGHTS

- Complexes $[\{SnR_3(OVp)\}_n]$, R = Me **(1)**, Bu **(2)** and Ph **(3)** have been prepared.
- Complexes **(1)** and **(3)** have been structurally authenticated.
- Complexes **(1)**–**(3)** have been studied by solution- and solid-state ^{119}Sn NMR.
- The biocide activity of **(1)**–**(3)** have been screened.

ARTICLE INFO

Article history:
Received 16 January 2015
Received in revised form 19 March 2015
Accepted 24 March 2015
Available online 8 April 2015

Keywords:
Biological activity
Organotin carboxylate
Structural determination

ABSTRACT

The reactions of triorganotin chlorides and sodium valproate, Na(OVp), yielded three triorganotin valproates $[\{SnMe_3(OVp)\}_n]$ **(1)**, $[\{SnBu_3(OVp)\}_n]$ **(2)** and $[SnPh_3(OVp)]$ **(3)**. All complexes have been authenticated in terms of infrared, ^{1}H and ^{13}C NMR, and solution- and solid-state ^{119}Sn NMR, ^{119}Sn Mössbauer and X-ray crystallography. The ^{119}Sn NMR experiments provided important informations concerning the structures of **(1)**–**(3)** in solution and in the solid state. The X-ray experiments revealed the double-polymeric chain of complex **(1)**, in which the geometry at the Sn(IV) is trigonal bipyramidal with intermolecular valproate bridges. The structure of complex **(3)** was re-determined and the new data show the tin cation at the centre of a distorted trigonal bipyramid, and not coordinated by four electron donating groups. The biological activity of all derivatives has been screened in terms of IC_{50} ($\mu mol\ L^{-1}$) against *C. albicans* (ATCC 18804), *C. tropicalis* (ATCC 750), *C. glabrata* (ATCC 90030), *C. parapsilosis* (ATCC 22019), *C. lusitaniae* (CBS 6936) and *C. dubliniensis* (clinical isolate 28). Complex **(3)** exhibited the best biocide activity.

Introduction

Tributyltin oxide (TBTO) was one of the first organotin compounds to be used as a biocide agent [1] in anti-fouling paints for ships [2,3]. However, important environmental problems led some nations to ban its use [4–7]. In spite of these drawbacks, organotins are among the most widely used organometallic compounds [8], and other potential applications have been discovered. In the 1970s the growth of malignant tumours was retarded by organotin carboxylates and aminoacids [9–14]. The antitumour activity of organotin complexes is still under investigation. In the last decades different biological applications of organotin complexes have been discovered. For example, Bu_2SnCl_2 or Ph_3SnCl can inhibit oedema in mice as effective as hydrocortisones [15,16]. Complexes with ligands derived from aminoquinolines have schizonticidal properties as antimalarial activities [17]. Those derivatives with some Schiff bases have potential use as amebicidal agents [18]. Some 2-alkylindole derivatives have been tested against *B. subtilis*, *B. pumilus*, *S.aureus* and *M. luteus* [19]. Activity against leshmaniasis in mice and helminthes in cats has been found for dioctyltin maleate [20,21]. Their complexes with 2,9-dimethyl-1,10-phenanthroline (Neocuproine) or with 3- and 4-aminobenzoic acids were tested towards human cervix

* Corresponding author. Tel.: +55 31 3409 5744; fax: +55 31 3409 5720.
E-mail address: gmlima@ufmg.br (G.M. de Lima).

http://dx.doi.org/10.1016/j.molstruc.2015.03.044
0022-2860/

carcinoma and leukemia K562. In the case of the former complexes they exhibited higher activities than cisplatin [22,23]. Therefore, it is quite significant that there is a wide range of applications and potential uses of organotin derivatives among other metal-derivatives, in fields such as agriculture, biology, catalysis, or organic synthesis [24]. Many works have described the preparation and characterization of organotin carboxylates [25–27] and their action against tumours, fungi, bacteria, and other microorganisms [1,28–31]. The number and nature of the organic groups bonded to the tin centre influence the toxicity towards microorganisms, which, in general, decreases in the order $R_3SnX > R_2SnX_2 > RSnX_3$. However, the order of toxicity depends on the microorganism, and varies from strain to strain [32]. It has been proposed that toxicity in the R_3Sn series correlates with total molecule surface (TSA) and hence *n*-propyl-, *n*-butyl-, *n*-pentyl-, phenyl-, and cyclohexyl-substituted tin should be more toxic than the ethyl- and methyl-containing derivatives. Moreover, the literature shows a correlation between toxicity and lipophilicity since the toxic effects of organotin complexes are intra-cellular as a consequence of the transport through the cell membrane [33]. Besides preparing new organotin-dithiocarbamates, investigating their potential applications [34] and screening their activity in the presence of some parasites [35] we have been interested in the mechanism of action of such complexes in biological media [36,37]. The effects of organotin dithiocarbamate or carboxylates on the cellular activity of some variety of *C. albicans* revealed no changes in DNA integrity or in the mitochondria function. However, all complexes reduced the ergosterol biosynthesis. Special techniques used for morphological investigations such as scanning electron microscopy (SEM) and transmission electron microscopy (TEM) suggested that the organotin complexes act on the cell membrane, in view of the observed cytoplasm leakage and strong deterioration of the cellular membrane [36,37]. Complexes **(1)**–**(3)** have been prepared earlier [38]. In the present work we have performed a deeper NMR study, in solution and in the solid state, correlating the results with those obtained from other spectroscopic techniques. In addition we have carried out the structural authentication of complexes **(1)**, and the chemical structure of **(3)** has been reviewed. The antifungal activity of the complexes has been screened in the presence of *C. albicans* (ATCC 18804), *C. tropicalis* (ATCC 750), *C. glabrata* (ATCC 90030), *C. parapsilosis* (ATCC 22019), *C. lusitaniae* (CBS 6936) and *C. dubliniensis* (Clinic isolate 28).

Experimental

Chemistry

Materials and instruments

All starting materials were purchased from Aldrich, Alfa Aesar, Fluka, Merck, Vetec or Synth and used as received. NMR spectra in solution were recorded at 200 MHz using a Bruker DPX-200 spectrometer equipped with an 89 mm wide-bore magnet. NMR spectra in solid state were recorded at 400 MHz using a Bruker Advance III DPX-400 spectrometer equipped with an 89 mm wide-bore magnet.^{1}H and ^{13}C{^{1}H} shifts are reported relative to $SiMe_4$ and ^{119}Sn{^{1}H} shifts relative to $SnMe_4$. The infrared spectra were recorded with samples pressed as KBr pellets on a Perkin–Elmer 238 FT-IR spectrometer in the range of 4000–400 cm^{-1}. Carbon and hydrogen analyses were performed on a Perkin–Elmer PE-2400 CHN equipment using tin sample-tubes. Tin analyses were performed on a Hitachi Z-8200 spectrometer. ^{119}Sn Mössbauer spectra were obtained in standard equipment at liquid nitrogen temperature using a $BaSnO_3$ source kept at room temperature. Intensity data for the X-ray study were collected on a Xcalibur, Atlas, Gemini, Kα/Mo (λ = 0.7107 Å). Data collection, reduction and cell refinement were performed using the CrysAlis RED program [39]. The structures were solved and refined employing the SHELXS-97 [40]. Further details are given in Table 3. All non-H atoms were refined anisotropically. The H atoms were refined with fixed individual displacement parameters [Uiso (H)Z1.2 Ueq (C)] using the SHELXL riding model. The ORTEP-3 program for windows [41] was used in the preparation of Figs. 4 and 5, sketched employing the Mercury program [42].

Syntheses

*Synthesis of [{$Me_3Sn(OVp)$}$_n$] **(1)***: To a round bottom flask (250 mL) charged with Na(OVap) (1.00 g, 6.02 mmol) in EtOH (100 mL) was added $SnMe_3Cl$ (1.24 g, 6.02 mmol) dissolved in 20 mL of EtOH. After 5 h of stir and reflux, the reaction vessel was left to settle down, and NaCl was separated by filtration. The solvent was removed in vacuum and the remaining white solid was recrystallized in a mixture of CH_2Cl_2/MeOH/H_2O (10:10:1) yielding X-ray quality crystals of **(1)**. Yield 62%. Mp 114.8–117.3 °C. IR (cm^{-1}): 1556 (ν_{as} CO_2^-), 1409 (ν_s CO_2^-), 477 (ν Sn—O). ^{1}H NMR (δ, $CDCl_3$): 2.32 {$O_2CC\underline{H}(CH_2CH_2CH_3)_2$}, 1.63–1.17 {$O_2CCH(C\underline{H}_2C\underline{H}_2CH_3)_2$}, 0.87{$^3J_{^1H4-^1H5}$ = 7.0 Hz} {$O_2CCH(CH_2CH_2C\underline{H}_3)_2$}, 0.50 $\left\{^2J_{(^{119}Sn-^1H)} = 57.3\ Hz\right\}$ {$Sn(C\underline{H}_3)_3$}; ^{13}C NMR (δ, $CDCl_3$): 182.5 {$O_2\underline{C}CH(CH_2CH_2CH_3)_2$}, 46.0 {$O_2C\underline{C}H(CH_2CH_2CH_3)_2$}, 35.4 {$O_2CCH(\underline{C}H_2CH_2CH_3)_2$}, 21.0 {$O_2CCH(CH_2\underline{C}H_2CH_3)_2$}, 14.3 {$O_2CCH(CH_2CH_2\underline{C}H_3)_2$}, −2.3 $\left\{^1J_{(^{119}Sn-^{13}C)} = 401\ Hz\right\}$ and $\left\{^1J_{(^{117}Sn-^{13}C)} = 383\ Hz\right\}$ {$Sn(\underline{C}H_3)_2$}.^{119}Sn NMR (δ, $CDCl_3$) 123.6 (weak) and −128.3 (strong). ^{119}Sn MAS NMR (δ_{iso}, 13 kHz): −34.9. ^{119}Sn Mössbauer, δ (mm s^{-1}) 1.29; Δ (mm s^{-1}) 3.47. Elemental analysis for $C_{11}H_{24}O_2Sn$ (MW 307.02 g mol^{-1}) found(calc): C 43.08 (43.03); H 7.90 (7.88); Sn 37.96 (38.67).

*Synthesis of [{$Bu_3Sn(OVp)$}$_n$] **(2)***: Prepared in a similar manner using Na(OVp), (1.00 g 6.02 mmol) and $SnBu_3Cl$ (2.04 g, 6.02 mmol). Yield 58%. Mp 51.2–53.4 °C. IR (cm^{-1}): 1574 m (ν_{as} CO_2^-), 1401 m (ν_s CO_2^-), 408 (ν Sn–O). ^{1}H NMR (δ, $CDCl_3$): 2.33 {$O_2CC\underline{H}(CH_2CH_2CH_3)_2$}, 1.78–1.02 {$O_2CCH(C\underline{H}_2C\underline{H}_2CH_3)_2$}, 0.85 {$O_2CCH(CH_2CH_2C\underline{H}_3)_2$}, 1.78–1.02 {$Sn(C\underline{H}_2C\underline{H}_2C\underline{H}_2CH_3)_3$}, 0.87 {$Sn(CH_2CH_2CH_2C\underline{H}_3)_3$}; ^{13}C NMR ($\delta$, $CDCl_3$): 182.2 {$O_2\underline{C}CH(CH_2CH_2CH_3)_2$}, 46.0 {$O_2C\underline{C}H(CH_2CH_2CH_3)_2$}, 35.4 {$O_2CCH(\underline{C}H_2CH_2CH_3)_2$}, 21.0 {$O_2CCH(CH_2\underline{C}H_2CH_3)_2$}, 14.2 {$O_2CCH(CH_2CH_2\underline{C}H_3)_2$}, 16.5 {$^1J_{(^{119}Sn-^{13}C)}$ = 361 Hz and $^1J_{(^{117}Sn-^{13}C))}$ = 345 Hz}, {$Sn(\underline{C}H_2CH_2CH_2CH_3)_3$}, 28.0 $\left\{^2J_{(^{119}Sn-^{13}C)} = 21.1\ Hz\right\}$ {$Sn(CH_2\underline{C}H_2CH_2CH_3)_3$}, 27.1 $\left\{^3J_{(^{119}Sn-^{13}C)} = 63.2\ Hz\right\}$ {$Sn(CH_2CH_2\underline{C}H_2CH_3)_3$}, 13.8 {$Sn(CH_2CH_2CH_2\underline{C}H_3)_3$}. ^{119}Sn NMR ($\delta$, $CDCl_3$) 100.2 (weak) and −153.4 (strong). ^{119}Sn MAS NMR (δ_{iso}, 13 kHz): −27.6. ^{119}Sn Mössbauer δ (mm s^{-1}) 1.41, Δ (mm s^{-1}) 3.52. Elemental analysis for $C_{20}H_{42}O_2Sn$ (MW 433.26 g mol^{-1}) found (calc) C 55.85 (55.44); H 9.80 (9.77); Sn 26.77 (27.40).

*Synthesis of [$Ph_3Sn(OVp)$] **(3)***: Similarly prepared using $SnPh_3Cl$ (2.44 g, 6.02 mmol) and sodium valproate, [Na(OVp)] (1.00 g, 6.02 mmol). Yield 67%. Mp 90.3–91.9 °C. IR (cm^{-1}): 1634 (ν_{as} CO_2^-); 1429 (ν_s CO_2^-); 444 (ν Sn–O). ^{1}H NMR (δ, $CDCl_3$): 7.96–7.48 {$Sn(C_6\underline{H}_5)_3$}; 2.60 {$O_2CC\underline{H}(CH_2CH_2CH_3)_2$}, 1.79–1.21 {$O_2CCH(C\underline{H}_2C\underline{H}_2CH_3)_2$}, 0.90 $\left\{^3J_{(^1H4-^1H5} = 7.1\ Hz\right\}$ {12H, $O_2CCH(CH_2CH_2C\underline{H}_3)_2$}; ^{13}C NMR ($\delta$, $CDCl_3$): 183.8 {$O_2\underline{C}CH(CH_2CH_2CH_3)_2$} 45.3 {$O_2C\underline{C}H(CH_2CH_2CH_3)_2$}; 35.2 {$O_2CCH(\underline{C}H_2CH_2CH_3)_2$}; 20.8 {$O_2CCH(CH_2\underline{C}H_2CH_3)_2$}; 14.2 {$O_2CCH(CH_2CH_2\underline{C}H_3)_2$}; 138.8 {$^1J_{(^{119}Sn-^{13}C)}$ = 648 Hz and $^1J_{(^{117}Sn-^{13}C)}$ = 619 Hz} {$Sn(\underline{C}_6H_5)_3$};137.0 $\left\{^2J_{(^{119}Sn-^{13}C)} = 48.1\ Hz\right\}$ {$Sn(\underline{C}_6H_5)_3$}; 129 $\left\{^3J_{(^{119}Sn-^{13}C)} = 63.1\ Hz\right\}$ {$Sn(\underline{C}_6H_5)_3$}; 130.2 {$Sn(\underline{C}_6H_5)_3$}. ^{119}Sn NMR (δ, $CDCl_3$): −116.9.

^{119}Sn MAS NMR (δ_{iso}, 10 kHz): −99.0; ^{119}Sn Mössbauer δ (mm s^{-1}): 1.24; Δ (mm s^{-1}): 2.22. Elemental analysis for $C_{26}H_{30}O_2Sn$ (MW = 493.23 g mol^{-1}): found (calc) C 63.11 (63.31); H 5.99 (6.13); Sn 23.97 (24.07).

Biological tests

The *in vitro* biocide activity of the starting materials and complexes **(1)**–**(3)** were screened against *C. albicans* (ATCC 18804), *C. tropicalis* (ATCC 750), *C. glabrata* (ATCC 90030), *C. parapsilosis* (ATCC 22019), *C. lusitaniae* (CBS 6936) and *C. dubliniensis* (Clinic isolate 28), according to the Gupta and Zacchino method [43]. Fungal strains were grown in Sabouraud Dextrose Broth (SDB) and then incubated for 24 horas at 37 °C. The concentration of the microorganisms was kept in the range of 1–2 × 10^8 cfu mL^{-1} (determined by the McFarland scale, cfu = colony forming unit), by spectrophotometric method. Different DMSO solutions of the complexes, starting materials and of nystatin and miconazole nitrate were prepared with concentration of 12.5 μg mL^{-1}. The MIC_{50} values were determined using an ELISA (BioTek) tray reader at a fixed wavelength of 490 nm.

Results and discussions

Chemistry

The complexes [{SnMe$_3$(OVp)}$_n$] **(1)**, [{SnBu$_3$(OVp)}$_n$] **(2)** and [SnPh$_3$(OVp)] **(3)** were obtained according to Scheme 1. They have been isolated as colourless and crystalline solids and their purity was attested in terms of the satisfactory melting points, or by C, H and Sn elemental analysis.

Infrared results

Information of $\Delta\nu_{COO}^{-}$ (ν_{as}–ν_s) values is important to provide details about the Sn-carboxyl bonding scheme [44–46]. We have found $\Delta\nu_{COO}^{-}$ at 138 cm^{-1} (ν_{as} = 1554 cm^{-1}; ν_s = 1416 cm^{-1}) for the Na(OVp). Only one stretching frequency was detected in the infrared spectra of complexes **(1)**–**(3)** [ν_{as} = 1556 cm^{-1}, ν_s = 1409 cm^{-1} **(1)**; ν_{as} = 1574 cm^{-1}, ν_s = 1401 cm^{-1} **(2)**; [ν_{as} = 1634 cm^{-1}, ν_s = 1429 cm^{-1} **(3)**]. Therefore, the following values of $\Delta\nu_{COO}^{-}$ were observed at 147, 173 cm^{-1} and 205 cm^{-1}, for **(1)**–**(3)** respectively, corroborating to the presence of bridging carboxylates, as confirmed by the X-ray crystallography experiments [36,47]. The presence of strong Sn–O bands in the region of 477–408 cm^{-1} was also detected.

Table 1
NMR data for complexes **(1)**–**(3)**.

Attribution	[{SnMe$_3$(OVp)}$_n$] **(1)**	[{SnBu$_3$(OVp)}$_n$] **(2)**	[SnPh$_3$(OVp)] **(3)**
H2	2.32 (m, 1H)	2.33 (m, 1H)	2.60 (m, 1H)
H3, H3′	1.63–1.17 (m, 8H)	1.78–1.02 (m, 26H)	1.79–1.21 (m, 26H)
H4, H4′	1.63–1.17 (m, 8H)	1.78–1.02 (m, 26H)	1.79–1.21 (m, 26H)
H5, H5′	0.87 (t, 9H) {^3J = 7.0 Hz}	0.85 (t, 15H)	0.90 (t, 6H) {^3J = 7.1 Hz}
Hα	0.50 (t, 9H) {^2J = 57.3 Hz}	1.78–1.02 (m, 26H)	–
Hβ, Hβ′	–	1.78–1.02 (m, 26H)	7.96–7.48 (m, 15H)
Hγ, Hγ′	–	1.78–1.02 (m, 26H)	7.96–7.48 (m, 15H)
Hδ	–	0.87 (t, 15H)	7.96–7.48 (m, 15H)
C1	182.5	182.2	183.8
C2	46.0	46.0	45.3
C3	35.4	35.4	35.2
C4	21.0	21.0	20.8
C5	14.3	14.2	14.2
Cα	−2.3 {^1J = 401/383 Hz}	16.5 {^1J = 361/345 Hz}	138.8 {^1J = 648/619 Hz}
Cβ, Cβ′	–	28.0 {^2J = 21.1 Hz}	137.0 {^2J = 48.1 Hz}
Cγ, Cγ′	–	27.1 {^3J = 63.2 Hz}	129.0 {^3J = 63.1 Hz}
Cδ	–	13.8	130.2

NMR results

The ^{1}H NMR experiments revealed the presence of one valproate group coordinated to each organotin fragment, in view of the obtained patterns for complexes **(1)**–**(3)**, Table 1.

The main interest in the ^{13}C NMR spectra concerns the resonance of the carboxylate group, and those of the Sn–R carbon atoms. The δ ($^{13}CO_2^-$) signal in the ligand remains almost unchanged in complexes **(1)**–**(3)**. Only one resonance was detected in the ^{13}C NMR experiments of complex **(1)**, at δ −2.3, with the corresponding $^1J_{(^{119}Sn-^{13}C)}$ and $^1J_{(^{117}Sn-^{13}C)}$ coupling constants detected at 401 and 383 Hz, respectively. The C_α, C_β, C_γ and C_δ chemical shifts assigned to the butyl group and phenyl moiety of complex [{SnBu$_3$(OVp)}$_n$] **(2)** and [SnPh$_3$(OVp)] **(3)** were identified at δ

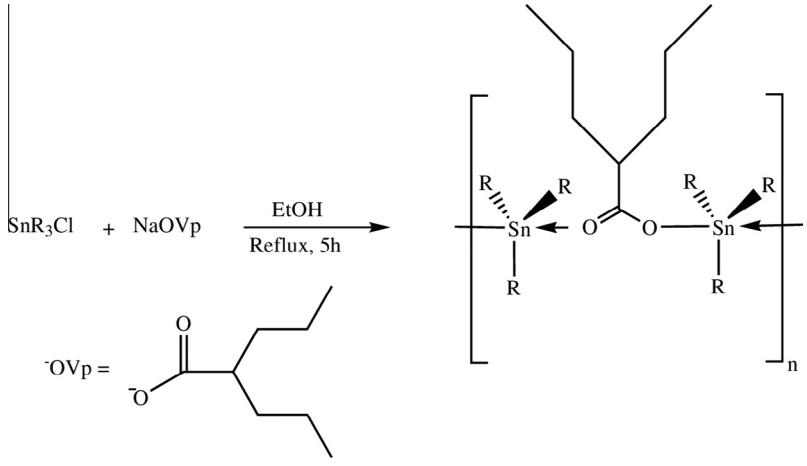

Scheme 1. Synthetic details of the preparation of complexes **(1)**–**(3)**.

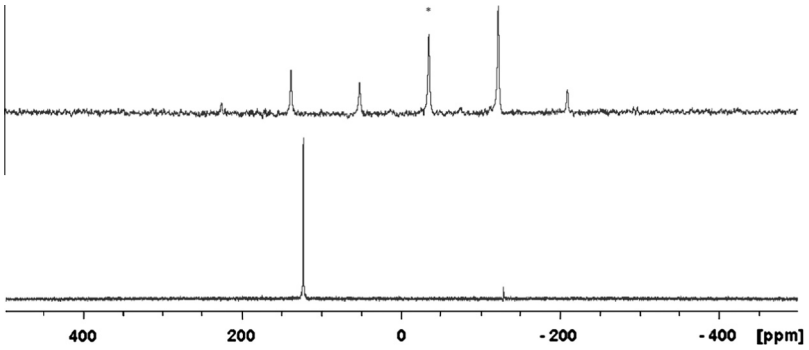

Fig. 1. Solid- and solution-state ^{119}Sn NMR spectra of [{$SnMe_3$(OVp)}$_n$] **(1).**

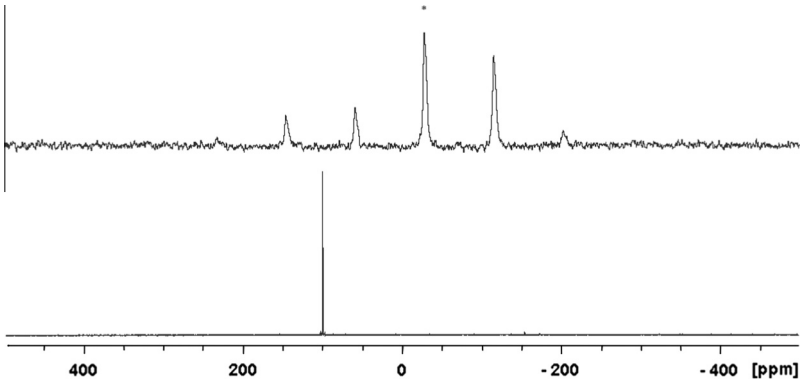

Fig. 2. Solid- and solution-state ^{119}Sn NMR spectra of [{$SnBu_3$(OVp)}$_n$] **(2).**

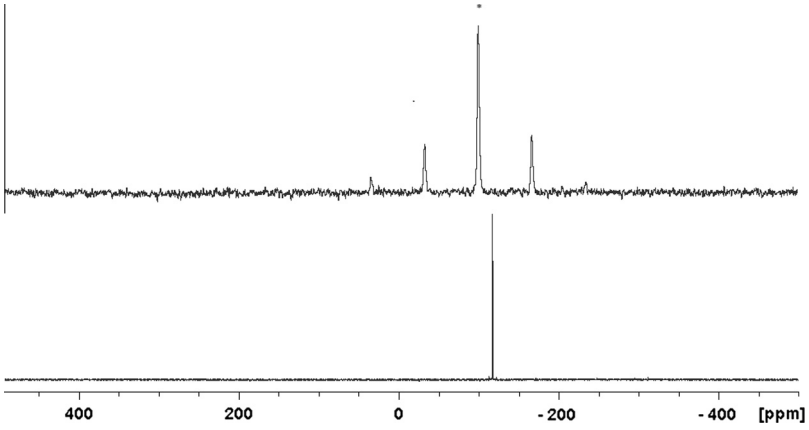

Fig. 3. Solid- and solution-state ^{119}Sn NMR spectra of [{$SnPh_3$(OVp)}] **(3).**

Table 2
Solid-state ^{119}Sn NMR data for complexes **(1)**–**(3)**.

Compound	$\delta_{in\ solution}$	$\delta_{iso\ obs}$	δ_{11}	δ_{22}	δ_{33}	$\delta_{iso\ calc}$	Ω	κ	$\Delta\delta$	η
[{$SnMe_3$(OVp)}$_n$] **(1)**	123.6, −128.3	−34.9	−169.80	−169.80	235.0	−34.88	404.8	−1.0	269.8	0.0
[{$SnBu_3$(OVp)}$_n$] **(2)**	100.2, −153.4	−27.6	−141.5	−141.5	198.0	−28.3	339.5	−1.0	226.3	0.0
[$SnPh_3$(OVp)] **(3)**	−116.9	−99.0	−204.5	−144.1	21.6	−99.0	226.1	−0.20	120.6	0.75

16.5, 27.1, 28.0 and 13.8, for **(2)**, and at $\underline{\delta}$ 138.8, 129.0, 137.0, and 130.2, for **(3)**. For complex **(2)** the ^{119}Sn–^{13}C coupling constants were: $^1J_{(^{119}Sn-^{13}C)} = 361$, $^1J_{(^{117}Sn-^{13}C)} = 345$, $^2J_{(^{117}Sn-^{13}C)} = 21.1$, and $^3J_{(^{119}Sn-^{13}C)} = 63.2$ Hz. On the other hand for **(3)** they were: $^1J_{(^{119}Sn-^{13}C)} = 648$, $^1J_{(^{117}Sn-^{13}C)} = 619$, $^2J_{(^{119}Sn-^{13}C)} = 48.1$ and $^3J_{(^{119}Sn-^{13}C)} = 63.1$ Hz. The coupling constants $^1J_{(^{119}Sn-^{13}C)}$ and $^2J_{(^{119}Sn-^{1}H)} = 361$ allow the evaluation of the C–Sn–C angle (θ) of the organotin fragment in solution. The literature suggests that ^1J

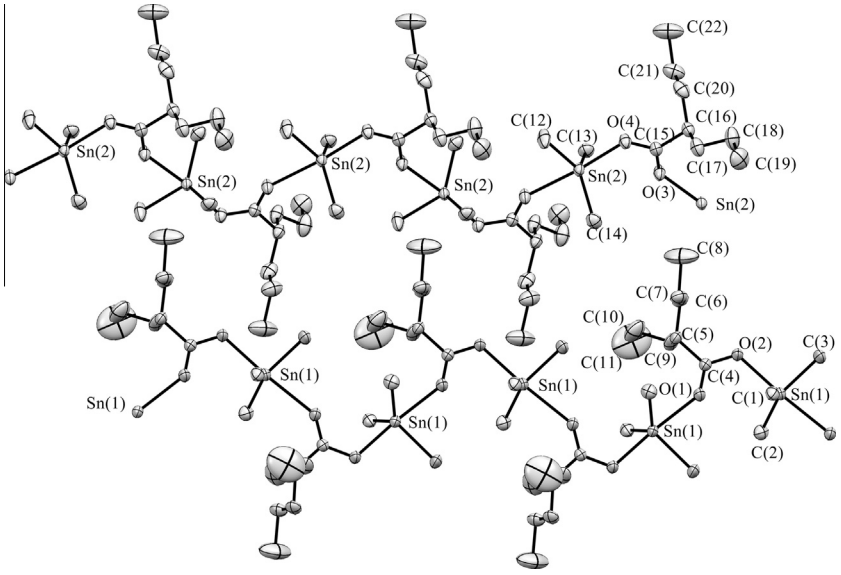

Fig. 4. The molecular structure of [{$SnMe_3(OVp)$}$_n$] **(1).**

and ^2J are very sensitive to variations in the coordination number. Empirical equations express a mathematical relationship between θ and $^1J_{(^{119}Sn-^{13}C)}$ for organotin complexes [48–50]:

$$|\,^1J_{(^{119}Sn-^{13}C)}| = 11.4(\theta) - 875) \text{ for methyl-possessing derivatives} \quad (1)$$

$$|\,^1J_{(^{119}Sn-^{13}C)}| = [(15.56 \pm 0.84)(\theta) - (1160 \pm 101) \text{ for phenyl-containing derivatives} \quad (2)$$

$$|\,^1J_{(^{119}Sn-^{13}C)}| = [(9.99 \pm 0.73)(\theta) - (746 \pm 100) \text{ for butyl-containing complexes} \quad (3)$$

The interpretation of chemical shifts and coupling constants in solution is generally based on crystal structure data (X-ray), therefore subject to uncertainties arising from solvation and dynamic effects. Eqs. (1)–(3) provide, with reasonable accuracy, means of determining the C–Sn–C angle in solution by measuring J coupling parameters. The average of the C–Sn–C angles obtained by the $^1J_{(^{119}Sn-^{13}C)}$ couplings were: 111.9° for **(1)**, 110.8° for **(2)** and 116.2° for **(3)**. The values observed in the X-ray experiments were 119.7° for **(1)** and 113.1° for **(3)**. The angles obtained for complex **(3)**, in the solid state, are close to those identified by ^{119}Sn NMR experiments in solution, differing from the values obtained for complex **(1)**. Therefore the $^1J_{(^{119}Sn-^{13}C)}$ coupling analyses suggest contrasting structures of complex **(1)** in solution and in the solid-state. On the other hand complex **(3)** displays similar structural arrangements, in view of the close values of C–Sn–C angle in solution 116.2° and in the solid state 113.1°. Although the crystallographic structure of **(2)** has not been solved, the obtained data suggest similarities with that of complex **(1)**.

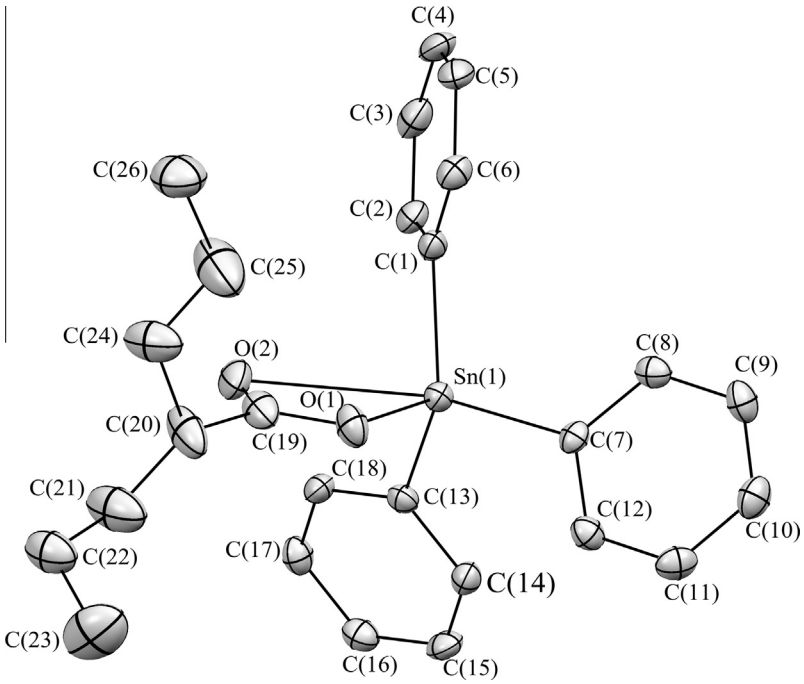

Fig. 5. The molecular structure of [{$SnPh_3(OVp)$}] **(3).**

The ^{119}Sn NMR spectrum of [{$SnMe_3(OVp)$}$_n$] **(1)** in solution, Fig. 1, revealed a major signal at δ 123.61 and a small one at −128.26. The same pattern was noticed for [{$SnBu_3(OVp)$}$_n$] **(2)**: δ 100.2 $\left\{{}^1J_{(^{119}Sn-^{13}C)} = 361\ Hz\right\}$ and −153.4 (very small signal), Fig. 2. ^{119}Sn MAS NMR experiments revealed signals at δ_{iso} −36 (10 kHz) or −34.9 (13 kHz) for **(1)** and δ_{iso} −29.4 (10 kHz) or −27.6 (13 kHz) for **(2)** (Fig. 3).

The disagreement in the ^{119}Sn NMR chemical shifts confirms that the solution- and the solid-state structures of **(1)** and **(2)** are quite different. The X-ray crystallographic study of **(1)** revealed a polymeric double chain motif. Therefore the chemical shifts observed in the ^{119}Sn MAS NMR spectra can be assigned to this polymeric structure, and in view of the single signals, the Sn(IV) nuclei in each chain are chemically and magnetically equivalent, as confirmed by the ^{119}Sn Mössbauer results. Therefore, the solution- and the solid-state structure of **(2)** and **(1)** might be similar. The two signals in the solution ^{119}Sn spectra of **(1)** and **(2)** result from the collapse of the polymeric chain either by the elongation of the extended Sn — O bonds or by forming monomers. Earlier reports in the literature discuss the ^{119}Sn NMR data of organotin carboxylates. In one of them the ^{119}Sn chemical shifts of Bu_3SnOAc were obtained at δ 123.1 and δ_{iso} −47 [51]. In another one the ^{119}Sn signal of $Me_3Sn(O_2CMe)$ was observed at δ_{iso} −27 [52]. These ^{119}Sn chemical shifts are very close to those obtained in our work. The structures of Bu_3SnOAc and $Me_3Sn(O_2CMe)$ was correctly assigned as monomeric with a tetracoordinated Sn(IV) atom in solution, and in the solid state they were wrongly interpreted as being trigonal bipyramidal rather than polymeric. In our work each solution- and the solid-state ^{119}Sn NMR spectra of [$SnPh_3(OVp)$] **(3)** showed a single signal, at δ −116.9 $\{{}^1J_{(^{119}Sn-^{13}C)} = 646$ and $^2J_{(^{119}Sn-^{13}C)} = 49.9\}$ and at δ_{iso} −98.9 (8 kHz), −99.0 (10 kHz), respectively, Table 2. The X-ray crystallographic study revealed a monomeric structure where the Sn(IV) atom lies at the centre of a distorted trigonal bipyramid, quite different from **(1)** and **(2)**. Therefore it confirms that the structure of complex **(3)** remains unchanged in solution. The ^{119}Sn MAS NMR experiments did not show the $J_{(^{119}Sn-^{13}C)}$ coupling constants of complexes **(1)**–**(3)**.

^{119}Sn Mössbauer spectroscopic results

The ^{119}Sn-Mössbauer parameter obtained in the previous work [38] revealed two pairs of signals for complexes **(1)** and **(2)**, showing the existence of more than one tin site in each complex [38]. The X-ray crystallographic study of **(1)** has shown two independent crystallographic arrangements, which are identical from the NMR point of view. In our work only one Sn site was found for **(1)** and **(2)** in the experiments, in accordance with the solid state ^{119}Sn NMR data. The structure and the corresponding ^{119}Sn parameters of the organotin precursors used in this work are as follows: [$SnPh_3Cl$] {tetrahedral, δ = 1.34 mm s^{-1} and Δ = 2.46 mm s^{-1}}, [53]; [$SnBu_3Cl$] {tetrahedral, δ = 1.58 mm s^{-1} and Δ = 3.40 mm s^{-1}} [54]; [$SnMe_3Cl$] {distorted trigonal bipyramid (at 135 K), δ = 1.47 mm s^{-1} and Δ = 3.32 mm s^{-1}}, [55]. Upon complexation we have observed the following parameters for the complexes, [{$SnMe_3(OVp)$}$_n$] **(1)**, δ = 1.29 mm s^{-1} and Δ = 3.47 mm s^{-1}; [{$SnBu_3(OVp)$}$_n$] **(2)**, δ = 1.41 mm s^{-1} and Δ = 3.52 mm s^{-1}; [$SnPh_3(OVp)$] **(3)**, δ = 1.24 mm s^{-1} and Δ = 2.22 mm s^{-1}. These values are closely related to those found in the literature for complexes **(1)**–**(3)**, however the geometry assigned to the complexes in the previous work is not supported by the ^{119}Sn-Mössbauer data. Although the solid state structure of [$SnMe_3Cl$] sketches a trigonal bipyramid with long and weak Sn···Cl intermolecular contacts, 3.259 Å, we have detected reduced isomer shift, δ, upon complexation, δ = 1.47 mm s^{-1}, [$SnMe_3Cl$], δ = 1.29 mm s^{-1}, **(1)**, suggesting a decrease in the *s* electron density contribution to the frontier orbitals in **(1)**. This reduction in δ might be a consequence of the replacement of a weak Sn···Cl by a strong Sn–O bond. In the starting materials the Sn atomic orbitals might have more sp^3 character than in **(1)**, with more sp^{3}d nature. So the structure of **(1)** is closer to a distorted bipyramidal trigonal geometry, as determined by X-ray experiments in our work, diverging from the results discussed in the literature [38]. We believe there is also a disagreement concerning the ^{119}Sn Mössbauer discussion of complexes **(2)** and **(3)**, which explains the reduction in the isomer shift parameter in both complexes in the solid state. For complexes **(1)**–**(3)** we have obtained the quadrupolar splitting at 3.47, 3.52 and 2.22 mm s^{-1}, very close to those values of the organotin precursors 3.32, 3.40 and 2.46 mm s^{-1}, indicating little changes in the symmetry of charge at the tin centre upon complexation.

X-ray crystallographic results

Biocide performance of organotin complexes relies upon subtle structural arrangements in solution or in the solid state, therefore structural authentication plays a key role in the understanding of the biocidal activity. The X-ray crystallographic study of complex **(1)** revealed an infinite double-polymeric chain structure, where

Table 3
The crystallographic parameters of the structural determination of complexes **(1)** and **(3)**.

Compound	**(1)**	**(3)**
Empirical formula	$C_{22}H_{48}O_4Sn_2$	$C_{26}H_{30}O_2Sn$
Formula weight	613.98	493.19
Temperature, K	270	120
Wavelength, Å	0.71073	0.71073
Crystal system	Monoclinc	Triclinic
Space group	P21/n	P1
a, Å	18.2357 (10)	9.778 (5)
b, Å	9.6847 (2)	9.904 (5)
c, Å	18.5295 (10)	13.710 (5)
α, °	90	98.577 (5)
β, °	112.696 (6)	109.663 (5)
γ, °	90	107.667 (5)
Volume, Å^3	3019.0 (2)	1143.9 (9)
Z	8	2
Calculated density, Mg m^{-3}	1.351	1.432
Absorption coefficient, mm^{-1}	1.67	1.14
F(000)	1248	504
Crystal size, mm	0.27 × 0.09 × 0.05	0.31 × 0.11 × 0.05
Theta range of data coll., °	2.0–26.37	2.3–26.37
Limiting indices	$h = -22 \rightarrow 22$ $k = -12 \rightarrow 12$ $l = -23 \rightarrow 23$	$h = -12 \rightarrow 12$ $k = -12 \rightarrow 12$ $l = -17 \rightarrow 17$
Reflections collected	30662	16201
Independent reflections	6174 [*R*(int) = 0.074]	4686 [*R*(int) = 0.053]
Reflections obd	4078	3986
Completeness	100%	100%
Absorption correction	Analytical	Analytical
Refinement method	Full-matrix least-squares on F2	Full-matrix least-squares on F2
Data/restrains/parameters	6174/0/253	4686/0/264
Goodness-of-fit on F^2	1.05	
Final R indices	0.0435	0.0391
[$I > 2\sigma(I)$]	*wR*2 = 0.1001	*wR*2 = 0.0801
R indices	0.0814 *wR*2 = 0.1299	0.0522 *wR*2 = 0.0871
Largest diff. peak and hole	0.70 and −1.08	1.62 and −0.94
CCDC Ref.	1042665	1042664

Table 4
Selected bond length and angles of complexes **(1)** and **(3)**.

Compound	Selected bond lengths (Å)		Selected angles (°)	
[{$SnMe_3(OVp)$}$_n$] **(1)**	Sn(1)–O(1)^{i}	2.395 (4)	O(2)–Sn(1)–O(1)^{i}	175.95 (15)
	Sn(1)–O(2)	2.185 (4)	C(1)–Sn(1)–C(3)	115.6 (3)
	Sn(1)–C(1)	2.115 (7)	C(2)–Sn(1)–C(1)	116.6 (3)
	Sn(1)–C(2)	2.106 (7)	C(2)–Sn(1)–C(3)	126.8 (3)
	Sn(1)–C(3)	2.150 (6)	O(4)–Sn(2)–O(3)^{ii}	174.62 (15)
	Sn(2)–O(3)^{ii}	2.381 (4)	C(13)–Sn(2)–C(12)	116.6 (4)
	Sn(2)–O(4)	2.180 (4)	C(13)–Sn(2)–C(14)	126.3 (3)
	Sn(2)–C(12)	2.139 (7)	C(14)–Sn(2)–C(12)	115.8 (4)
	Sn(2)–C(13)	2.096 (8)		
	Sn(2)–C(14)	2.109 (8)		
[$SnPh_3(OVp)$] **(3)**	Sn(1)–O(1)	2.063 (3)	O(1)–Sn(1)′-C(1)	110.81 (16)
	Sn(1)–O(2)	2.788(4)	O(1)–Sn(1)′–C(7)	95.86 (15)
	Sn(1)–C(1)	2.125 (4)	O(1)–Sn(1)′–C(13)	108.93 (15)
	Sn(1)–C(7)	2.127 (4)	C(1)–Sn(1)–C(7)	112.60 (16)
	Sn(1)–C(13)	2.132 (4)	C(1)–Sn(1)–C(13)	116.79 (16)
			C(7)–Sn(1)–C(13)	109.83 (17)

Symmetry codes: **(1)**: (i) $-x+3/2, y+1/2, -z+3/2$; (ii) $-x+5/2, y-1/2, -z+3/2$; (iii) $-x+3/2, y-1/2, -z+3/2$; (iv) $-x+5/2, y+1/2, -z+3/2$.
(2): (i) $-x, -y, -z$.

the anionic valproate binds two tin centres *via* bridging carboxylates, Table 3 and Fig. 4. Each chain possesses a tin cation surrounded by three methyl **(1)** groups and two oxygen atoms, outlining an almost perfect trigonal bipyramidal geometry. The equatorial corners are occupied by the organic groups and the axial positions by the oxygen atoms. The small differences in the two chains relate to little changes in the Sn–O and Sn–C bonds. In both chains the Sn cation is asymmetrically bonded to a CH_3 group and to oxygen electron-donor centres. In one chain these bonds are Sn(1)–O(1) 2.395 (4) and Sn(1)–O(2) 2.185 (4) Å, Sn(1)–C(1) 2.115 (7), Sn(1)–C(2) 2.106 (7) and Sn(1)–C(3) 2.150 (6)Å; and in the other one they are as follows: Sn(2)–O(3) 2.381 (4) and Sn(2)–O(4) 2.180 (4) Å, Sn(2)–C(12) 2.139 (7), Sn(2)–C(13) 2.096 (8) and Sn(2)–C(14) 2.109 (8) Å. The angles C–Sn–C and O–Sn–O are all close to 120° and 180° as expected for trigonal bipyramidal geometry slightly distorted, Table 4 [56]. The O–Sn–O is nearly linear at the tin, O(2)–Sn(1)–O(1) 175.95(15)° and O(4)–Sn(2)–O(3) 174.62 (15)° but bent at the oxygen, imposing a zig–zag character to the polymeric backbone. Sn–O associations connecting the two chains might be neglected.

In view of the minor conflicts regarding the ^{119}Sn Mössbauer study between our work and that reported previously [38] we have re-determined the crystallographic structure of complex **(3)**, Fig. 5. The crystallographic data are roughly the same with little modifications, however we have observed that the longer Sn–O bond is shorter than the summation of the Sn and O Van der Waals radii, 3.69 Å. This highlights a strong covalent contribution to this interatomic contact, not considered in the previous work [38]. Therefore the coordination number of the complex is 5 rather than 4, and the most likely geometry at the Sn cation emerges from the distortion of a square pyramid or a trigonal bipyramid. The valproate ligand is asymmetrically bonded to the tin atom through the oxygen electron donor centres, Sn–O(1) 2.063 (3) Å and Sn–O(2), 2.788 (3) Å. The Sn–C bonds, Sn–C(1) 2.125 (4), Sn–C(13) 2.132 and Sn–C(7) 2.137 (4) Å are longer than the same bonds in the Ph_3SnCl, 2.113, 2.114 and 2.120 Å [57]. The C–Sn–C angles, C(1)–Sn–C(7), 119.6 (16)°, C(1)–Sn–C(13), 116.79 (16)°, and C(7)–Sn–C(13), 109.83 (17)°, are slightly different of those angles observed in the Ph_3SnCl [51].

Biocide assay results

Metal-containing drugs alone or in combination with pharmaceuticals in clinical use might represent a way to overcome resistance of microbes to antibiotics. In this work the biocide assays were performed in terms of inhibitory concentrations, which are more consistent and reliable. A pre-screening against *C. albicans*, *C. tropicalis*, *C. glabrata*, *C. parapsilosis*, *C. lusitaniae* and *C. dubliniensis* has been performed with complexes **(1)**–**(3)** in a concentration of 250 μg mL^{-1}, according to a pre-established protocol [58]. Experiments of IC_{50} were only performed for those complexes with more than 50% inhibition growth of the studied microorganism. The antifungal activities of the complexes [{$SnMe_3(OVp)$}$_n$], **(1)**, [{$SnBu_3(OVp)$}$_n$] **(2)** were similar to those of the organotin halides, Me_3SnCl and Bu_3SnCl. Complex **(3)**, [$SnPh_3(OVp)$] displayed smaller MIC in comparison to Ph_3SnCl in the presence of all fungi, except toward the colonies of *C. grabata* and *C. parapsilosis*. However these results must be carefully considered in view of the high toxicity normally displayed by organotin halides. These compounds are easily hydrolysed, forming hydroxides or oxides which are even more toxic to mammals or to the environment. As observed in Table 5, the organotin valproates were generally better biocide agents than nystatin, but poorer than miconazole nitrate, which exhibited lower MIC values than **(1)**–**(3)**. Among all complexes **(1)** was the least effective and it was only active in

Table 5
Minimal Inhibition Concentration (MIC) (mmol L^{-1}) for complexes **(1)**–**(3)**, for the starting organotin halides and for the control drugs.

IC_{50} mmol L^{-1}	*C. albicans*	*C. tropicalis*	*C. glabrata*	*C. parapsilosis*	*C. lusitaniae*	*C. dubliniensis*
[{$SnMe_3(OVp)$}$_n$] **(1)**	821.5	–	–	407.3	–	–
[{$SnBu_3(OVp)$}$_n$] **(2)**	0.335	1.35	3.7	2.8	0.119	0.385
[$SnPh_3(OVp)$] **(3)**	0.298	0.548	2.8	4.3	0.096	0.084
Me_3SnCl	649	–	–	1142	–	–
Bu_3SnCl	0.266	0.452	2.8	2.5	0.035	0.136
Ph_3SnCl	0.382	0.772	2.0	2.8	0.226	0.246
Nystatin	19.2	51.4	11.0	23.6	22.6	8.3
Miconazole	0.202	0.288	0.8	0.00045	<0.0000062	<0.0000062

the presence of *C. albicans* and *C. parapsilosis*, with MIC concentrations of 821.5 and 407.3 mol L^{-1}, respectively.

Following the same tendency observed for organotin complexes published in the literature the triphenyl derivative complex **(3)** exhibited the better biocide activity in comparison to the other complexes [59]. The biological activity of organotin complex depends on a series of properties such as lipophilic/hydrophilic that balances the transport of the compound across the cell membranes, or the affinity between the organotin fragments and the target site. A closer structural and biocide activity is observed for organotin complexes. Lipophilicity is an important and critical physical property that affects the bioavailability of organotin complexes. For this class of complexes this property grows with an increase of the organic group attached to the tin centre. So, it might explain the reason that triorganotin-possessing fragments exhibit the best antifungal activity.

Conclusions

Cases of resistance of microorganisms to conventional treatment as well as the toxicity of medicaments justify the search for alternative drugs and the study of their mechanisms of action. The synthesis, characterization and biological aspects of $[\{SnMe_3(OVp)\}_n]$ **(1)**, $[\{SnBu_3(OVp)\}_n]$ **(2)** and $[SnPh_3(OVp)]$ **(3)** have been the focus of this report. ^{13}C and ^{119}Sn couplings served to conclude that the structure of **(1)** and **(2)** in solution are quite different from those in the solid state. Therefore solvation and dynamic processes in solution might not be neglected. However, complex **(3)** does not change too much on going from solid to solution. In addition the complexes have been characterized by IR, ^{119}Sn Mössbauer spectroscopy, and X-ray diffraction for complexes **(1)** and **(3)**. Some disagreement has emerged in comparing our results with those found in a recent paper. Four species of fungus, *C. albicans*, *C. tropicalis*, *C. glabrata*, *C. parapsilosis*, *C. lusitaniae and C. dubliniensis*, have been cultivated in the presence of complexes **(1)**–**(3)**. In terms of IC_{50}, complex **(1)** is poorly active and displayed low antifungal activity in the presence of *C. albicans* and *C. parapsilosis*. Complexes **(2)** and **(3)** were more active than nystatin but less effective than miconazole nitrate. Complex **(3)** exhibited modest antifungal activity in the presence of the fungal species.

Supplementary data

Crystallographic data are available on request at Cambridge Crystallographic Data Centre on quoting the deposition numbers CCDC 1042665 **(1)** and 1042665 **(3)**.

Acknowledgements

This work was supported by CNPq and FAPEMIG – Brazil.

References

[1] C.J. Evans, R. Hill, J. Oil Colour Chem. Assoc. 64 (1998) 215.
[2] D. Liu, R.J. Maguire, Y.L. Lau, G.J. Pacepavicius, H. Okamaru, I. Aoyama, Water Res. 31 (1997) 2363.
[3] N. Voulvoulis, M.D. Scrimshaw, J.N. Lester, Appl. Organomet. Chem. 13 (1999) 135.
[4] R.J. Maguire, Water Qual. Res. J. Can. 26 (1991) 43.
[5] K. Frent, Crit. Rev. Toxicol. 26 (1996) 1.
[6] J. White, J.M. Tobin, J.J. Cooney, Can. J. Microbiol. 45 (1999) 541.
[7] B. Chantong, D.V. Kratschmar, A. Lister, A. Odermatt, Toxicol. Lett. 230 (2014) 177.
[8] K.E. Appel, Drug Metab. Rev. 36 (2004) 763.
[9] M. Sirajuddin, S. Ali, V. Mckee, M. Sohail, H. Pasha, Eur. J. Med. Chem. 84 (2014) 343.
[10] H.A. Meinema, A.M.J. Liebregts, H.A. Budding, E.J. Bulten, Rev. Silicon, Rev. Silicon, Germanium, Tin Lead Comp 8 (1985) 157.
[11] F. Arjmand, M. Muddassir, I. Yousuf, J. Photochem. Photobiol. B 136 (2014) 62.
[12] R. Barbieri, L. Pellerito, G. Ruisi, M.T. Lo Guidice, Inorg. Chim. Acta 66 (1982) L39.
[13] R. Barbieri, G. Ruisi, in: NATO Adv. Workshop on the Effect of Tin upon Malignant Cell Growth, Brussels, 1989, Abstr. PO_2.
[14] F. Huber, G. Roge, L. Carl, G. Atassi, F. Spreafico, S. Filippeschi, R. Barbieri, A. Silvestri, E. Rivarola, G. Ruissi, F. Di Branca, G. Alonzo, J. Chem. Soc., Dalton Trans. (1985) 523.
[15] Y. Arakawa, O. Wada, Biochem. Biophys. Commun. 125 (1989) 59.
[16] Y. Arakawa, O. Wada, Igaku no Agumi 136 (1986) 177.
[17] N. Wasi, H.B. Singh, A. Gajanana, A.N. Raichowdary, Inorg. Chim. Acta 135 (1987) 133.
[18] A.K. Saxena, J.K. Koacher, J.P. Tandon, S.R. Das, Toxicol. Environ. Health 10 (4–5) (1982) 709.
[19] A.K. Senigupta, A.A. Gupta, Ind. J. Chem. Sect. B (Org.-Med. Chem.) 22 (3) (1983) 263.
[20] W. Peters, E.R. Trotter, B.L. Robinson, Ann. Trop. Med. Parasitol. 74 (1980) 321.
[21] A.I. Tereeva, G.M. Borodina, Farmakol. Toksikol. 30 (1967) 207.
[22] M. Yousefi, M. Safari, M.B. Torbati, A. Amanzadeh, J. Struct. Chem. 55 (2014) 101.
[23] D. Tzimopoulos, I. Sanidas, A.C. Varvogli, A. Czapik, M. Gdaniec, E. Nikolakaki, P.D. Akrivos, J. Inorg. Biochem. 104 (2010) 423.
[24] A.G. Davies, M. Gielen, K.H. Pannell, E.R.T. Tiekink, Tin Chemistry – Fundamentals, Frontiers and Applications, Wiley, Chichester, 2008.
[25] H. Tlahuext, R. Reyes-Martinez, G. Vargas-Pineda, M. Lopez-Cardoso, H. Hopfl, J. Organomet. Chem. 696 (2011) 693.
[26] A. Husain, S.A.A. Nami, K.S. Siddiqi, J. Mol. Struct. 970 (2010) 117.
[27] J.P. Fuentes-Martinez, I. Toledo-Martinez, P. Roman-Bravo, P.G.Y. Garcia, C. Godoy-Alcantar, M. Lopez-Cardoso, H. Morales-Rojas, Polyhedron 28 (2009) 3953.
[28] A. Normah, K.N. Farahana, B. Ester, H. Asmah, N. Rajab, A.A. Halim, Res. J. Chem. Environ. 15 (2011) 544.
[29] R. Singh, N.K. Kaushik, Spectroc. Acta A 71 (2008) 669.
[30] E. Santacruz-Juarez, J. Cruz-Huerta, I.F. Hernandez-Ahuactzi, R. Reyes-Martinez, H. Tlahuext, H. Morales-Rojas, H. Hopfl, Inorg. Chem. 47 (2008) 9804.
[31] S. Shahzadi, S. Ali, M. Fettouhi, J. Chem. Crystallogr. 38 (2008) 273.
[32] J.S. White, J.M. Tobin, J.J. Cooney, Can. J. Microbiol. 45 (1999) 541.
[33] J.J. Cooney, S. Wuertz, J. Indust. Microbiol. 4 (1989) 375.
[34] D.C. Menezes, G.M. de Lima, A.O. Porto, M.P. Ferreira, J.D. Ardisson, R.A. Silva, Main Group Met. Chem. 30 (2007) 49.
[35] D.C. Menezes, G.M. de Lima, G.S. de Oliveira, A.V. Boas, A.M.A. Nascimento, F.T. Vieira, Main Group Met. Chem. 31 (2008) 21.
[36] D.C. Menezes, F.T. Vieira, G.M. de Lima, J.L. Wardell, M.E. Cortes, M.P. Ferreira, M.A. Soares, A.V. Boas, Appl. Organomet. Chem. 22 (2008) 221.
[37] D.C. Menezes, G.M. de Lima, F.A. Carvalho, M.G. Coelho, A.O. Porto, R. Augusti, J.D. Ardisson, Appl. Organomet. Chem. 24 (2008) 650.
[38] O. Pellerito, C. Prinzivalli, E. Foresti, P. Sabatino, M. Abbate, G. Casella, T. Fiore, M. Scopelliti, C. Pellerito, M. Giuliano, G. Grasso, L. Pellerito, J. Inorg. Biochem. 125 (2013) 16.
[39] G.M. Sheldrick, Acta Crystallogr. A 64 (2008) 112.
[40] G.M. Sheldrick, SHELXL-97. Program for Crystal Structure Refinement, University of Göttingen, Germany, 1997.
[41] L.J. Farrugia, J. Appl. Crystallogr. 30 (1997) 565.
[42] C.F. Macrae, P.R. Edgington, P. McCabe, E. Pidcock, G.P. Shields, R. Taylor, M.J. van De Streek, J. Appl. Crystallogr. 39 (2006) 453.
[43] A.S. Zacchino, M.P. Gupta, Manual de Técnicas in vitro Para la Detección de Compuestos Antifúngicos, Corpus Editorial y Distribuidora, Rosario, 2007.
[44] M. Nath, S. Pokharia, X. Song, G. Eng, M. Gielen, M. Kemmer, M. Biesemans, R. Willem, D. de Vos, Appl. Organomet. Chem. 17 (2003) 305.
[45] M.A. Abdellah, S.K. Hadjikakou, N. Hadjiliadis, M. Kubicki, T. Bakas, N. Kourkoumelis, Y.V. Simos, S. Karkabounas, M.M. Barsan, I.S. Butler, Bioinorg. Chem. Appl. (2009) 542979.
[46] A. Szorcsik, L. Nagy, J. Sletten, G. Szalontai, E. Kamu, T. Fiore, L. Pellerito, E. Kalman, J. Organomet. Chem. 689 (2004) 1145.
[47] G.B. Deacon, R.J. Phillips, Coord. Chem. Rev. 33 (1980) 227.
[48] J. Holecek, M. Nadvornik, K. Handlir, A. Lycka, J. Organomet. Chem. 315 (1986) 299.
[49] T.P. Lockhart, W.F. Manders, J.J. Zuckerman, J. Am. Chem. Soc. 107 (1985) 4546.
[50] T.P. Lockhart, W.F. Manders, J. Am. Chem. Soc. 109 (1987) 7015.
[51] C.H. Yoder, R.A. Morreall, C.I. Butoi, W.J. Kowalski, J.N. Spencer, J. Organomet. Chem. 448 (1993) 59.
[52] J. Kummerlen, A. Sebald, Solid State Nucl. Mag. Res. 3 (1994) 137.
[53] J.S. Tse, F.L. Lee, J. Gabe, Acta Cryst. C C42 (1986) 1876.
[54] P.J. Smith, Organomet. Chem. Rev. A 5 (1970) 373.
[55] S. Calogero, P. Ganis, V. Peruzzo, G. Tagliavini, J. Organomet. Chem. 179 (1979) 145.
[56] V. Chandrasekhar, P. Thilagar, P. Sasikumar, J. Organomet. Chem. 691 (2006) 1681.
[57] J.S. Tse, F.L. Lee, E.J. Gabe, Acta Crystallogr. C 42 (1986) 1876.
[58] J.J. Cooney, S. Wuertz, J. Ind. Microbiol Biotechnol. 4 (2005) 375.
[59] W. Rehman, J. Khan, B. Muhammad, S.W.H. Shah, R. Rashid, Mini. Rev. Med. Chem. 12 (2012) 426.